

Article

Synthesis, Characterization, and Electrochemical Behavior of $\text{LiMn}_x\text{Fe}_{(1-x)}\text{PO}_4$ Composites Obtained from Phenylphosphonate-Based Organic-Inorganic Hybrids

Alessandro Dell'Era ^{1,2,*}, Mauro Pasquali ¹, Elvira Maria Bauer ², Stefano Vecchio Cipriotti ^{1,*} , Francesca A. Scaramuzzo ¹  and Carla Lupi ³

¹ Department of Basic and Applied Sciences for Engineering (SBAI), Sapienza University of Rome, Via del Castro Laurenziano 7, 00161 Rome, Italy; mauro.pasquali@uniroma1.it (M.P.); francesca.scaramuzzo@uniroma1.it (F.A.S.)

² Istituto di Struttura della Materia ISM—CNR, Via Salaria, km. 29.300, C.P. 10, 00015 Rome, Italy; elvira.bauer@ism.cnr.it

³ Department Chemical Engineering Materials Environment DICMA, University Sapienza Rome, Via Eudossiana 18, 00184 Rome, Italy; carla.lupi@uniroma1.it

* Correspondence: alessandro.dellera@uniroma1.it (A.D.); stefano.vecchio@uniroma1.it (S.V.C.); Tel.: +39-064-976-6906 (S.V.C.)

Received: 14 November 2017; Accepted: 27 December 2017; Published: 30 December 2017

Abstract: The synthesis of organic-inorganic hybrid compounds based on phenylphosphonate and their use as precursors to form $\text{LiMn}_x\text{Fe}_{(1-x)}\text{PO}_4$ composites containing carbonaceous substances with sub-micrometric morphology are presented. The experimental procedure includes the preliminary synthesis of Fe^{2+} and/or Mn^{2+} phenylphosphonates with the general formula $\text{Fe}_{(1-x)}\text{Mn}_x[(\text{C}_6\text{H}_5\text{PO}_3)(\text{H}_2\text{O})]$ (with $0 < x < 1$), which are then mixed at different molar ratios with lithium carbonate. In this way the carbon, obtained from in situ partial oxidation of the precursor organic part, coats the $\text{LiMn}_x\text{Fe}_{(1-x)}\text{PO}_4$ particles. After a structural and morphological characterization, the electrochemical behavior of lithium iron manganese phosphates has been compared to the one of pristine LiFePO_4 and LiMnPO_4 , in order to evaluate the doping influence on the material.

Keywords: lithium-ion battery; $\text{LiMn}_x\text{Fe}_{(1-x)}\text{PO}_4$; carbon coating; pseudo-diffusion coefficient; potential step voltammetry; electrochemical impedance spectroscopy

1. Introduction

Nowadays, lithium-ion batteries are the most developed energy sources for modern portable electronics and their use in automotive application is also increasing [1–8]. So far, several materials, such as LiCoO_2 and LiMn_2O_4 , have been used as cathode, but recently LiFePO_4 has attracted researchers' interest due to its high specific energy, which may reach 580 Wh/kg, and relatively low production cost [9–14]. As a drawback, LiFePO_4 has low ionic diffusivity and conductivity [15–17], which limits its use as cathode. The electronic conductivity of LiFePO_4 can be enhanced by using several materials processing methods such as in situ carbon synthesis, or by particle coating with conductive carbons [18], or by an ion doping approach [19–24]. In the latter case, the oxidized form of LiFePO_4 should be modified with cations having ionic radius slightly higher than Fe^{2+} and Fe^{3+} , such as manganese, facilitating a wider channel for lithium-ion diffusion, increasing the mobility of lithium ion but, at the same time, avoiding the structure to be stressed [25]. Moreover, the LiFePO_4 particles size should be reduced to decrease the average free lithium pathway in insertion/de-insertion process

and raise the performances. Indeed, in this way, all the material can be effectively used, consequently enhancing the specific capacity. The aim of this work has been to analyze the electrochemical performance of lithium iron phosphate with the addition of manganese $\text{LiMn}_x\text{Fe}_{(1-x)}\text{PO}_4$ starting from Fe^{2+} and Mn^{2+} phenylphosphonates (general formula $\text{Fe}[(\text{C}_6\text{H}_5\text{PO}_3)(\text{H}_2\text{O})]$ or $\text{Mn}[(\text{C}_6\text{H}_5\text{PO}_3)(\text{H}_2\text{O})]$) in appropriate ratio as metal-organic precursor and Li_2CO_3 as inorganic precursor. Moreover, in order to verify possible differences in the electrochemical performances, one of the lithium iron manganese phosphates, i.e., $\text{LiFe}_{0.9}\text{Mn}_{0.1}\text{PO}_4$, has been also synthesized by using the precursor $\text{Fe}_{0.9}\text{Mn}_{0.1}[(\text{C}_6\text{H}_5\text{PO}_3)(\text{H}_2\text{O})]$. Thermal, structural, and morphological analyses have been performed on both precursors and final materials; finally, an electrochemical characterization has been carried out on all prepared samples to evaluate if the synthesis process and the hetero-metal adding degree can influence their specific capacity.

2. Materials and Methods

2.1. Synthesis of Precursors

Analytical grade (Sigma Aldrich Chemical Co., Darmstadt, Germany) phenylphosphonic acid ($\text{H}_2\text{C}_6\text{H}_5\text{PO}_3$), ammonium hydroxide (NH_4OH), iron(II) sulphateheptahydrate ($\text{FeSO}_4 \cdot 7\text{H}_2\text{O}$), and manganese(II) sulphatemonohydrate ($\text{MnSO}_4 \cdot \text{H}_2\text{O}$) were used for the synthesis without further purification. HPLC (High Pressure Liquid Chromatography) water (Carlo Erba, Milan, Italy) was used as a solvent. Usual Schlenk techniques were used to prepare the phenylphosphonate precursor materials.

All metal(II) phosphonate precursors, i.e., $\text{Fe}_{0.9}\text{Mn}_{0.1}(\text{C}_6\text{H}_5\text{PO}_3)(\text{H}_2\text{O})$ (**P1**), $\text{Fe}[(\text{C}_6\text{H}_5\text{PO}_3)\text{H}_2\text{O}]$ (**P2**) and $\text{Mn}(\text{C}_6\text{H}_5\text{PO}_3)(\text{H}_2\text{O})$ (**P3**), were obtained following the synthetic procedure described previously for iron(II) phenylphosphonate monohydrate $\text{Fe}[(\text{C}_6\text{H}_5\text{PO}_3)\text{H}_2\text{O}]$ [21,22]: 10 g (63.25 mmol) of $\text{H}_2\text{C}_6\text{H}_5\text{PO}_3$ were suspended under continuous stirring in 50 mL of water in a 100 mL two-necked flask (flask 1). NH_4OH (about 9.5 mL, 30% in H_2O) was added, up to $\text{pH} = 7$, to the white colloidal suspension obtained, thus giving the water soluble ammonium salt of the phenylphosphonic acid $(\text{NH}_4)_2(\text{C}_6\text{H}_5\text{PO}_3)$. In another 100 mL two-necked flask (flask 2), 7 g (25.17 mmol) of $\text{FeSO}_4 \cdot 7\text{H}_2\text{O}$ were dissolved in 35 mL of degassed water. After the complete dissolution of ferrous sulphate, the degassed aqueous solution of $(\text{NH}_4)_2(\text{C}_6\text{H}_5\text{PO}_3)$ was transferred from flask 1 to flask 2 under a stream of inert gas and with a filtration system. The filtration system guarantees the transfer of a filtered and clear solution of the ammonium salt of phenylphosphonic acid to iron(II) sulphate. During the transfer, iron(II) phenylphosphonate, $\text{Fe}[(\text{C}_6\text{H}_5\text{PO}_3)\text{H}_2\text{O}]$ formed instantaneously as a white flaked precipitate. The white colloidal suspension thus obtained was maintained under continuous stirring under flowing nitrogen for approx. 2 h ($\text{pH}_{\text{fin}} = 6.14$). The precipitate was then filtered in air, washed with water to neutrality with acetone, and finally air-dried. Three different metal(II) phenylphosphonate precursors, reported in Table 1, were isolated by the former preparation method.

Table 1. Molecular formulas of precursors.

Material	Formula
P1	$\text{Fe}_{0.9}\text{Mn}_{0.1}(\text{C}_6\text{H}_5\text{PO}_3)(\text{H}_2\text{O})$
P2	$\text{Fe}(\text{C}_6\text{H}_5\text{PO}_3)(\text{H}_2\text{O})$
P3	$\text{Mn}(\text{C}_6\text{H}_5\text{PO}_3)(\text{H}_2\text{O})$

2.2. Synthesis of $\text{LiMn}_{0.1}\text{Fe}_{0.9}\text{PO}_4$

In particular, $\text{LiMn}_{0.1}\text{Fe}_{0.9}\text{PO}_4$ was synthesized starting from different precursors following different procedures, and the final products obtained were compared in terms of morphology and electrochemical performances. In detail, $\text{LiMn}_{0.1}\text{Fe}_{0.9}\text{PO}_4$ was synthesized by mixing in a mechanical mill Li_2CO_3 (analytical grade by Sigma Aldrich Chemical Co.) and either the precursor **P1** $\text{Fe}_{0.9}\text{Mn}_{0.1}(\text{C}_6\text{H}_5\text{PO}_3)\cdot\text{H}_2\text{O}$ (sample **S1**) or the precursors **P2** $\text{Fe}(\text{C}_6\text{H}_5\text{PO}_3)\cdot\text{H}_2\text{O}$ and

P3 $\text{Mn}(\text{C}_6\text{H}_5\text{PO}_3)\cdot\text{H}_2\text{O}$ in molar ratio 0.9/0.1 (sample **S2**). After the grinding process the light-grey powder homogeneous mixture of the reagents was placed in an alumina crucible and transferred into the central zone of a tubular furnace for calcination. In order to maintain an inert environment, the mixture of reagents was degassed for 1 h at room temperature under nitrogen flowing. Successively the powder underwent a calcination at 600 °C for 16 h under nitrogen flowing. The calcined product was then cooled under inert gas to room temperature, thus obtaining a fine black powder.

2.3. Synthesis of $\text{LiMn}_x\text{Fe}_{(1-x)}\text{PO}_4$ (with $x = 0.05, 0.1, 0.5, 0.9$, and 0.95)

The synthesis was performed starting from Li_2CO_3 , **P2** and **P3** precursors, as described in the previous paragraph. In order to obtain all the desired compounds, **P2** and **P3** were mechanically mixed with a molar ratio (1– x): x respectively, where $x = 0.05, 0.1, 0.5, 0.9$, and 0.95, followed by thermal treatment under inert atmosphere as reported above.

3. Results and Discussion

3.1. Precursors Characterization

Infrared spectra of the different monohydrate precursors appear quite similar and present several bands, as shown in Figure 1. The bands between 3420 and 3470 cm^{-1} and the band at 1604 cm^{-1} correspond respectively to the stretching and bending vibrations of the water molecule of M(II) phenylphosphonate monohydrate ($\text{M} = \text{Fe}, \text{Mn}, \text{Fe}_{0.9}\text{Mn}_{0.1}$). Other characteristic bands of this compounds are located between 3074 and 3054 cm^{-1} and are associated with the stretching vibrations of the C-H bond of the phenyl group, while the band at 1438 cm^{-1} corresponds to C-C bond stretching of the same group. Finally, in the region between 1200–970 cm^{-1} , the characteristic stretching vibrations of the P-O bond of the anion $(\text{PO}_3)^{2-}$ are observed. The complete conversion of phenylphosphonic acid to metal(II) phosphonate is confirmed by the absence of the typical OH-binding strain vibrations of the P-OH group, generally observed as wide bands between 2900 and 2300 cm^{-1} .

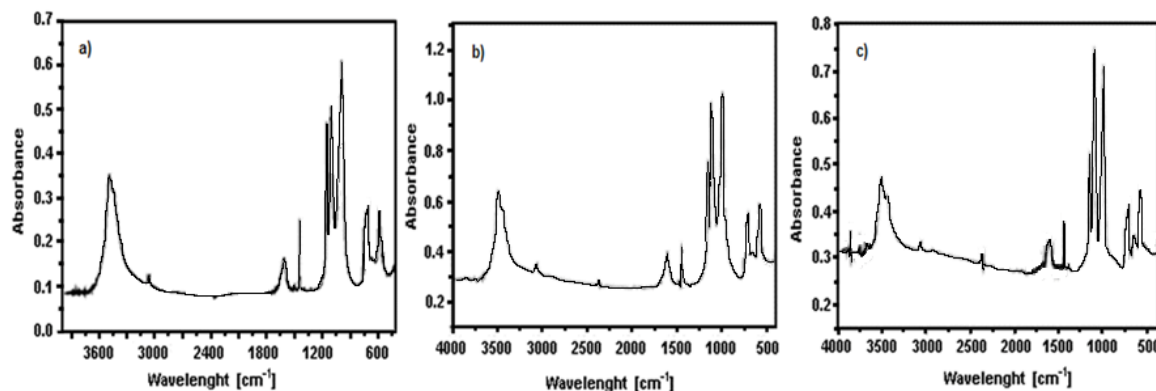


Figure 1. FT-IR spectra of precursors: (a) $\text{Fe}_{0.9}\text{Mn}_{0.1}(\text{C}_6\text{H}_5\text{PO}_3)(\text{H}_2\text{O})$ (**P1**); and (b) $\text{Fe}[(\text{C}_6\text{H}_5\text{PO}_3)\text{H}_2\text{O}]$ (**P2**) and (c) $\text{Mn}(\text{C}_6\text{H}_5\text{PO}_3)(\text{H}_2\text{O})$ (**P3**).

In Figure 2, the X-ray diffractograms and the refining results obtained by the Rietveld method are reported. The only crystalline phase present in the analyzed precursor powders corresponds to the expected M(II)phenylphosphonate ($\text{M} = \text{Fe}, \text{Mn}, \text{Fe}_{0.9}\text{Mn}_{0.1}$) [26,27]. All the three phenylphosphonate precursors crystallize in the orthorhombic spatial group $\text{Pmn}2_1$. In Table 2 the cell parameters for the different samples are reported. Excluding lattice parameter “ b ”, it is possible to state that passing from iron to manganese produces an increasing of the cell size.

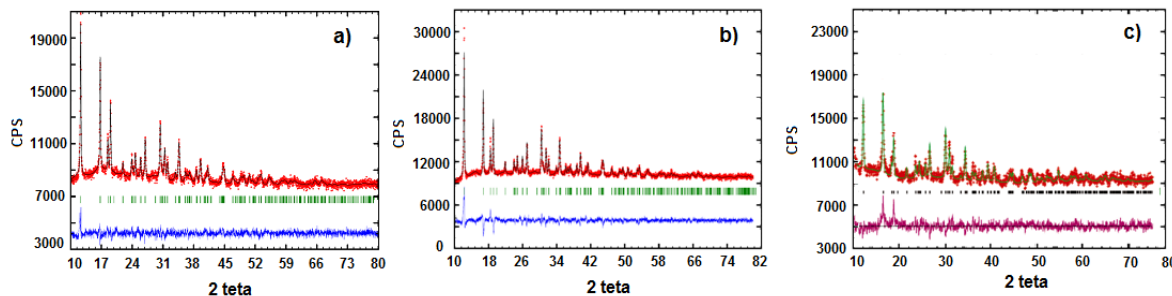


Figure 2. X-ray Diffraction pattern of precursors: (a) $\text{Fe}_{0.9}\text{Mn}_{0.1}(\text{C}_6\text{H}_5\text{PO}_3)(\text{H}_2\text{O})$ (**P1**); and (b) $\text{Fe}(\text{C}_6\text{H}_5\text{PO}_3)\cdot\text{H}_2\text{O}$ (**P2**) and (c) $\text{Mn}(\text{C}_6\text{H}_5\text{PO}_3)\cdot\text{H}_2\text{O}$ (**P3**).

Table 2. Lattice parameters of precursors (in Å), where $\alpha = \beta = \gamma = 90^\circ$.

Material (Symbol)	a	b	c
$\text{Fe}_{0.9}\text{Mn}_{0.1}(\text{C}_6\text{H}_5\text{PO}_3)\cdot\text{H}_2\text{O}$ (P1)	5.680	14.410	4.900
$\text{Fe}(\text{C}_6\text{H}_5\text{PO}_3)\cdot\text{H}_2\text{O}$ (P2)	5.652	14.404	4.882
$\text{Mn}(\text{C}_6\text{H}_5\text{PO}_3)\cdot\text{H}_2\text{O}$ (P3)	5.751	14.401	4.953

3.2. Characterization of $\text{LiFe}_{0.9}\text{Mn}_{0.1}\text{PO}_4$

DSC-TG (Differential Scanning Calorimetry–Thermo-Gravimetry) curves obtained under nitrogen flow for $\text{Fe}_{0.9}\text{Mn}_{0.1}(\text{C}_6\text{H}_5\text{PO}_3)\cdot\text{H}_2\text{O}$ (**P1**)/ Li_2CO_3 mixture (sample **S1**) and for $\text{Fe}(\text{C}_6\text{H}_5\text{PO}_3)\cdot\text{H}_2\text{O}$ (**P2**) and $\text{Mn}(\text{C}_6\text{H}_5\text{PO}_3)\cdot\text{H}_2\text{O}$ (**P3**) (**P2:P3 = 0.9:0.1**)/ Li_2CO_3 mixture (sample **S2**) are reported, respectively, in Figure 3a,b. The thermal behaviour of both mixtures resulted to be quite similar.

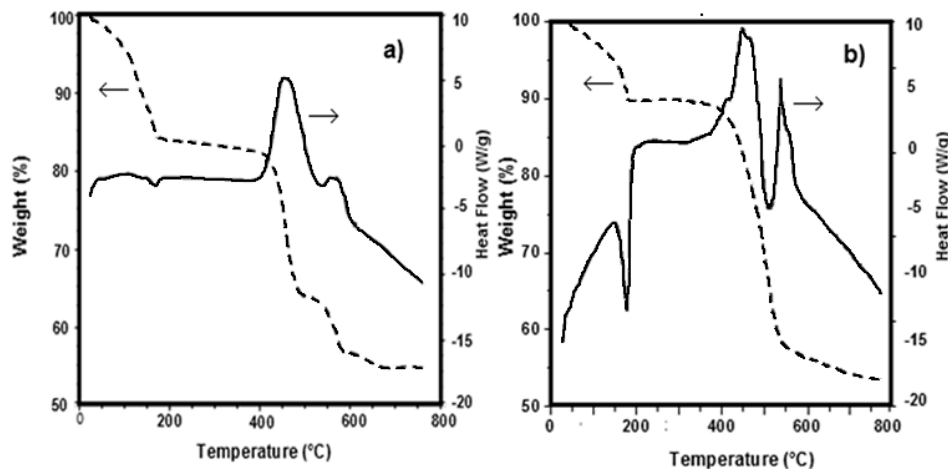


Figure 3. DSC-TG curves of: (a) sample **S1**: **P1**/ Li_2CO_3 ; and (b) sample **S2**: (**P2:P3 = 0.9:0.1**)/ Li_2CO_3 .

Part of the water, probably physically adsorbed on the sample, is lost at temperatures lower than 100°C . The remaining part, i.e., the crystallization water, is lost at about 200°C : this phenomenon is clearly highlighted by the end thermal peak observable in the DSC curves at 180°C . The weight loss up to 180°C is about 11–15%. At higher temperatures two exothermic effects are displayed in the DSC curves, namely at 400 and 550°C , which are accompanied by a weight loss in the TG curves of about 25–30% and 8–10%, respectively.

These effects are related to the decomposition of carbonate and organo-phosphonates and to the formation of lithium metal(II) phosphate. Such experimental evidences are in good agreement with literature, according with the dehydration of some hydrate metal phosphates which proceeds by both anion disproportion and condensation. The X-ray powder diffraction patterns of $\text{LiMn}_{0.1}\text{Fe}_{0.9}\text{PO}_4$

prepared from either **P1** and Li_2CO_3 or **P2, P3**, and Li_2CO_3 precursors are very alike as well, as shown in Figure 4. Both belong to orthorhombic space group *Pnma* (olivine like structure) [13]. The similarity between these two samples is evident also from SEM (Scanning Electron Microscopy) images reported in Figures 5 and 6.

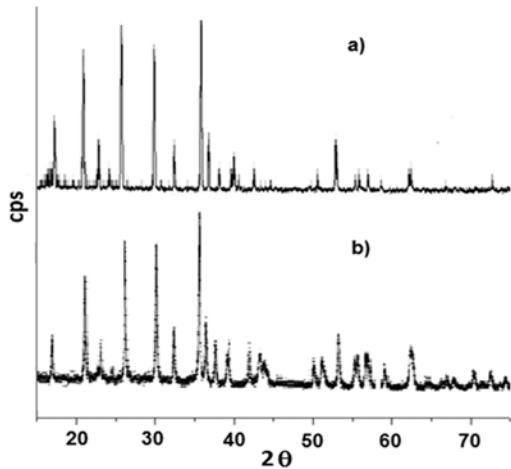


Figure 4. X-ray Diffraction pattern of $\text{LiFe}_{0.9}\text{Mn}_{0.1}\text{PO}_4$: (a) sample S1: $\text{P1}/\text{Li}_2\text{CO}_3$; and (b) sample S2: ($\text{P2}:\text{P3} = 0.9:0.1$)/ Li_2CO_3 .

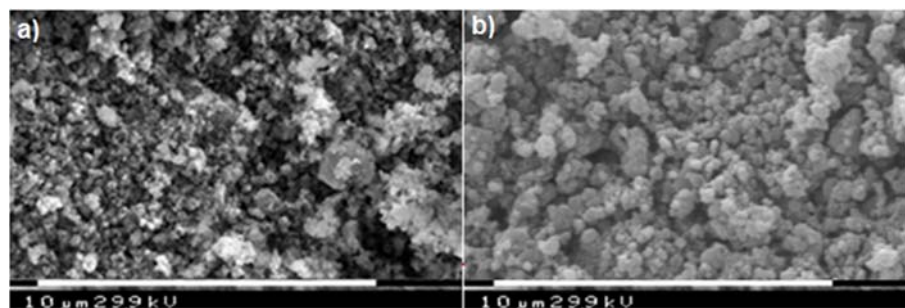


Figure 5. SEM images of $\text{LiFe}_{0.9}\text{Mn}_{0.1}\text{PO}_4$: (a) sample S1: $\text{P1}/\text{Li}_2\text{CO}_3$; and (b) sample S2: ($\text{P2}:\text{P3} = 0.9:0.1$)/ Li_2CO_3 .

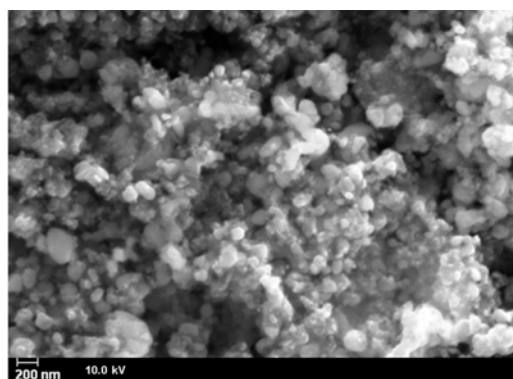


Figure 6. Morphology and size details at higher magnification.

The particles show a comparable morphology. In both samples the particles appear agglomerated and the presence of two phases can be noted: the former, likely carbon, is characterized by very small spheres, while the second one ($\text{LiMn}_{0.1}\text{Fe}_{0.9}\text{PO}_4$) is characterized by larger and less regular particles.

The particles are spheroidal, or in any case there is no dimension that prevails over the others during the growth, like for example in a needle structure; such experimental evidence suggests that during the thermal treatment strong nucleation with the formation of small nucleuses growing indifferently in all directions occurs. In Figure 6 a higher magnification highlights the formation of very small particles with nanometric size. Actually, the formation of carbon on the active material surface can inhibit the particle grow ensuring a tiny granulometry and possibly can provide good conductivity and electric contact between particles [13–28].

Electrochemical galvanostatic tests on both samples S1 and S2 are shown in Figure 7. The cathode electrodes have been charged and discharged with a current value of C/5 and a specific capacity of about 115–120 mAh/g has been obtained. The materials seem to show similar behaviour, even though sample S2, obtained by using P2, P3 and Li₂CO₃ precursors, presents higher capacity and seems to be more stable upon cycling. On the other hand, the synthesis by P1 precursor always produces a less performing material, even though it is not straightforward to give an explanation for such different behaviour. Several tests have been performed for each material, and the results are well reproducible.

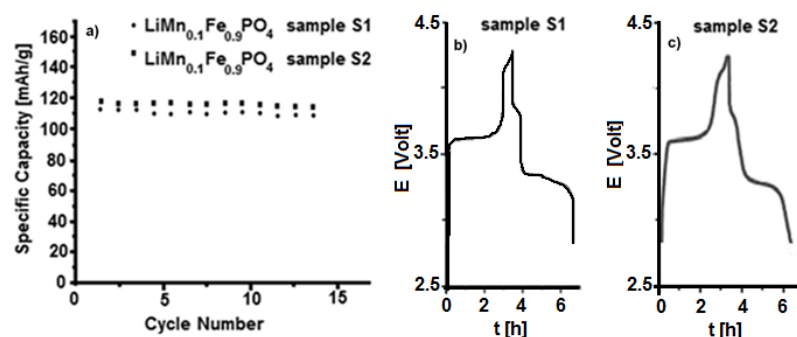


Figure 7. (a) Electrochemical galvanostatic tests at C/5 rate for samples S1 and S2; and (b) voltage profile of sample S1; (c) voltage profile of Sample S2.

3.3. Characterization of LiMn_xFe_(1-x)PO₄ (with x = 0, 0.05, 0.1, 0.5, 0.9, 0.95, and 1)

Furthermore, taking in consideration this electrochemical results, a series of LiMn_xFe_(1-x)PO₄ (with x = 0, 0.05, 0.1, 0.5, 0.9, 0.95 and 1), obtained only from P2 and/or P3 and Li₂CO₃ precursors, have been prepared and characterized.

The powder X-ray diffraction spectra of LiMn_xFe_(1-x)PO₄ (x = 0; 0.05; 0.1; 0.5; 0.9; 0.95; 1) are shown in Figure 8. As it can be observed, substituting manganese in lithium manganese phosphate with iron(II) slightly moves all peaks to the right, although the similarity of the crystalline structure of the two lithium metal(II) phosphates is clear.

Moreover, in Table 3 the refinement results for cell parameters and crystallites size T, calculated by Scherrer equation (T = 0.9λ/Δ(2θ) cosθ), have been reported and it is clear that passing from LiFePO₄ to LiMnPO₄ the cell size slightly increases, while the crystallites size decreases.

Table 3. Cell parameters and crystallite size.

Compound	a (Å)	b (Å)	c (Å)	Crystallite Size T (Å)
LiFePO ₄	10.330	6.010	4.690	393
LiFe _{0.95} Mn _{0.05} PO ₄	10.335	6.011	4.693	370
LiFe _{0.9} Mn _{0.1} PO ₄	10.347	6.020	4.699	368
LiFe _{0.5} Mn _{0.5} PO ₄	10.372	6.054	4.706	365
LiFe _{0.1} Mn _{0.9} PO ₄	10.448	6.103	4.743	282
LiFe _{0.05} Mn _{0.95} PO ₄	10.448	6.104	4.743	280
LiMnPO ₄	10.450	6.108	4.732	265

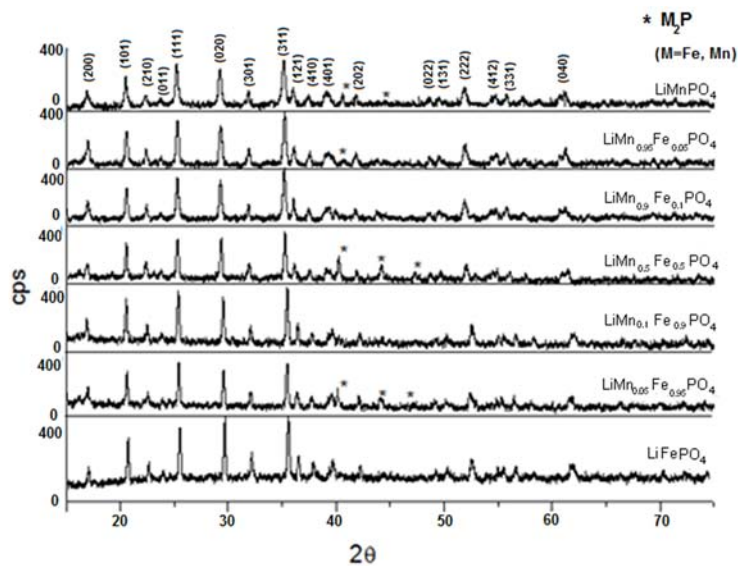


Figure 8. X-ray powder diffraction pattern of $\text{LiMn}_x\text{Fe}_{(1-x)}\text{PO}_4$ ($x = 0; 0.05; 0.1; 0.5; 0.9; 0.95; 1$).

In some samples ($x = 0.05; 0.5; 0.95; 1$) the presence of iron phosphide (Fe_2P) impurities have been detected. Replacement of the bivalent hetero-metal atom does not affect the crystalline structure of pure lithium iron and manganese phosphate. Indeed the crystalline structure (space group) is the same but substitution of iron with manganese (different atomic radius) in effect shifts the peak positions slightly and this is visible also in the reported XRD spectra. What is important here is that for all samples one, unique crystalline phase has been detected while the mechanic mixture clearly shows peak splitting due to the presence of two crystalline phases. On the other hand, when simply mixing together (0.5:0.5) LiMnPO_4 and LiFePO_4 , the observed X-ray diffractogram shows a splitting of the peaks, as reported in Figure 9. Actually, in this case two similar crystalline structures presenting slightly different peak positions are present, therefore, two distinct phases and a splitting of peaks are evident. It is worth to note that in the case of manganese-iron phosphate synthesized from metal(II) phenylphosphonate mixtures as described before, even when Mn(II) and Fe(II) are present in equal ratio, as in $\text{LiMn}_{0.5}\text{Fe}_{0.5}\text{PO}_4$, formation of only one crystalline phase has been observed.

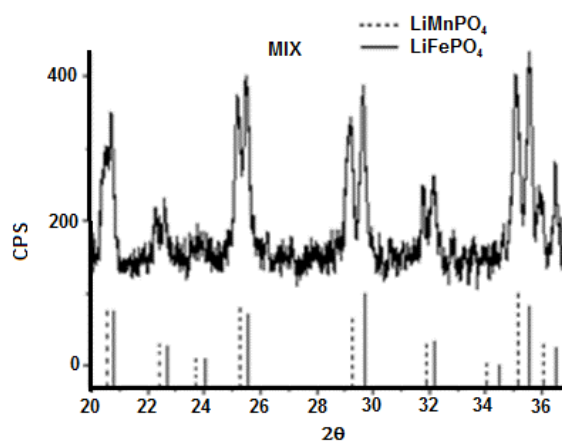


Figure 9. Comparison between X-ray Diffraction spectra of a binary mixture of LiFePO_4 and LiMnPO_4 and corresponding pure lithium metal phosphates.

The results of BET analysis for cathodic powders obtained are reported in Table 4 along with the carbon weight percentage determined by elemental analysis, which ranges from 10% to 13.7%.

This percentage value has been also confirmed by EDX analysis performed on some samples. The average specific surface is equal to about $115 \text{ m}^2 \cdot \text{g}^{-1}$.

Table 4. Specific surface of cathodic powder and carbon percentage.

Material (Symbol)	Specific Surface Area ($\text{m}^2 \cdot \text{g}^{-1}$)	Carbon Content (%)
LiFePO ₄	105	10.0
LiMn _{0.05} Fe _{0.95} PO ₄	100	10.2
LiMn _{0.1} Fe _{0.9} PO ₄	130	12.5
LiMn _{0.5} Fe _{0.5} PO ₄	115	10.3
LiMn _{0.9} Fe _{0.1} PO ₄	110	11.3
LiMn _{0.95} Fe _{0.05} PO ₄	151	13.7
LiMnPO ₄	105	11.5

The SEM images in Figure 10 show similarity of both morphology and particle size of the various samples. Indeed, identical considerations already done for LiMn_{0.1}Fe_{0.9}PO₄ and no particular differences can be highlighted.

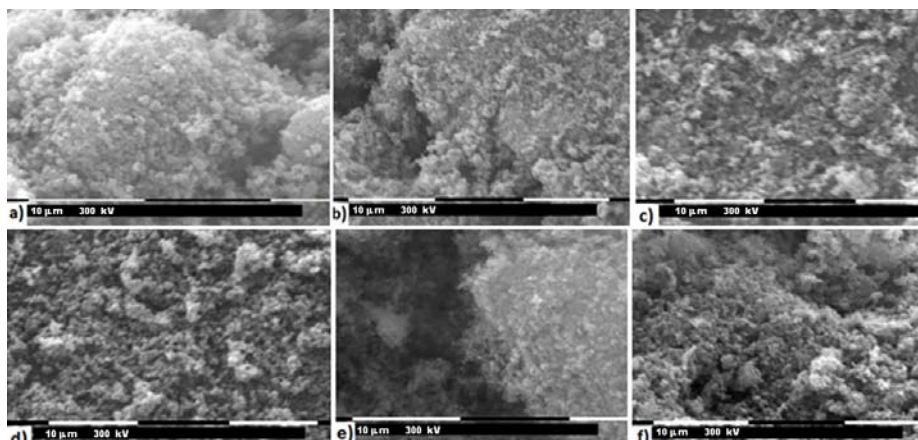


Figure 10. SEM images of: (a) LiFePO₄; (b) LiMn_{0.05}Fe_{0.95}PO₄; (c) LiMn_{0.5}Fe_{0.5}PO₄; (d) LiMn_{0.9}Fe_{0.1}PO₄; (e) LiMn_{0.95}Fe_{0.05}PO₄; and (f) LiMnPO₄.

The electrochemical tests indicate that pure lithium iron phosphate is the material with the highest specific capacity, i.e., about $150 \text{ mAh} \cdot \text{g}^{-1}$. Upon increasing of manganese content, the capacity gradually drops, reaching the significantly low value of $23 \text{ mAh} \cdot \text{g}^{-1}$ for LiMn_{0.95}Fe_{0.05}PO₄. Therefore, regarding the specific capacity, the presence of manganese does not seem to have particular advantages.

As it can be seen from Figure 11a, the only advantage shown by the presence of manganese is a higher insertion-deinsertion potential value. In fact, the potential value of the Mn³⁺/Mn²⁺ redox couple is 4.15 V, while for the Fe³⁺/Fe²⁺ redox couple it results to be 3.5 V, both vs. Li⁰/Li⁺.

The LiMn_{0.5}Fe_{0.5}PO₄ compound exhibits a poorly stability upon cycling, while the compounds with a higher percentage of manganese show a low capacities. Taking into consideration the two pure compounds, namely LiFePO₄ and LiMnPO₄, they both have capacity higher than the respective modified compounds. In particular, the presence of Mn(II) decreases the capacity of LiFePO₄ more than the substitution of manganese with iron in LiMnPO₄. Indeed the plateaus at 3.5 V for LiMn_{0.9}Fe_{0.1}PO₄ and LiMn_{0.95}Fe_{0.05}PO₄ are absent, while for LiMn_{0.5}Fe_{0.5}PO₄ the plateau at 3.5 V is shorter than the one at 4.15 V. Even if there is just one phase, as it is possible to note by XRD, lithium ion insertion into the structure induces either reduction of Fe⁺³ to Fe⁺² at about 3.5 V or the reduction of Mn⁺³ to Mn⁺² at about 4.1 V, producing in both cases an equilibrium between the oxidized and reduced form (namely, MePO₄/LiMePO₄, where Me is Fe or Mn), and then determining the stress inside the

structure. Such stress, produced by hetero-atom reduction, is even enhanced when its amount is very low, since, in this case, around its position dissimilar atoms are present and the redox reaction could be inhibited. However, the presence of low quantity of manganese can help the lithium insertion into the iron-base structure, but not vice versa.

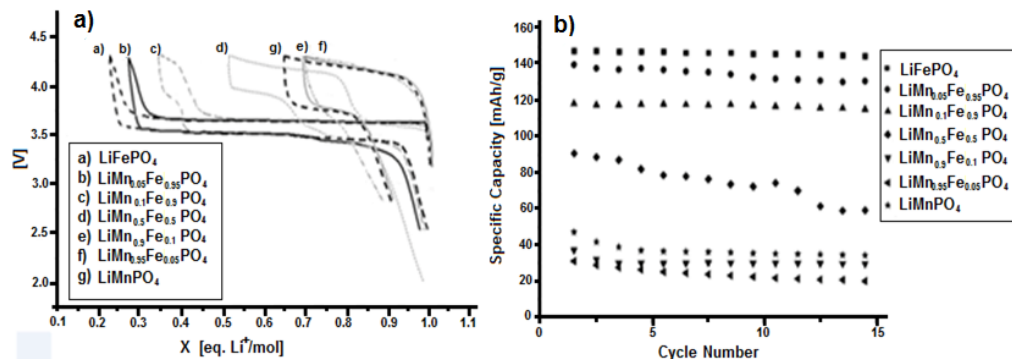


Figure 11. Results of tests at C/5 for $\text{LiMn}_x\text{Fe}_{(1-x)}\text{PO}_4$ ($x = 0.05; 0.1; 0.5; 0.9; 0.95$): (a) Charge-discharge curves; and (b) specific capacity.

Among the different compounds of the series, only those of lithium iron-phosphate with low manganese content have been taken into account for further investigation, since they have the highest capacities. To evaluate the performances of those samples, the reversibility degree of the insertion-deinsertion process, the pseudo-diffusion lithium coefficient and the charge transfer resistance, were calculated by PSV, PITT, and EIS experiments, respectively.

In Figure 12 potential step voltammetry is shown for LiFePO_4 , $\text{LiMn}_{0.05}\text{Fe}_{0.95}\text{PO}_4$, and $\text{LiMn}_{0.1}\text{Fe}_{0.9}\text{PO}_4$. In this picture, the insertion-deinsertion process can be observed in correspondence of two peaks. The upward peaks correspond to the oxidation process at approximately 3.47 V for all samples (odd sweeps), while the downward peaks represent the reduction process at approximately 3.37, 3.40, and 3.42 V (even sweeps) for LiFePO_4 , $\text{LiMn}_{0.05}\text{Fe}_{0.95}\text{PO}_4$, and $\text{LiMn}_{0.1}\text{Fe}_{0.9}\text{PO}_4$, respectively. In general terms, the shorter the distance between oxidation and reduction peaks, the higher the reversibility of the process. In the present case it is possible to recognize that manganese content in LiFePO_4 increases the process reversibility. The average value of pseudo-diffusion coefficient has been also evaluated determining the Cottrell region for the potential step voltammetry corresponding to the deinsertion process, by using the PITT technique [29–31], and assuming the average particle radius as the diffusion characteristic length, L, equal to about 0.1×10^{-4} cm. Indeed, as said before, the insertion of lithium takes place by means of several reaction fronts, and a pseudo-diffusivity coefficient should be more correctly defined, despite McKinnon and Hearing's assumption [32], who found that it is not possible to distinguish between two different diffusion models based on continuous (solid solution formation) or not continuous (two-phase formation) charging procedures. In Table 5 the pseudo-diffusion coefficient value for both pure LiFePO_4 and the materials with low manganese content has been reported. Increasing the manganese content, the value enhances very slightly, so that only few changes can be reached with manganese adding.

Impedance spectroscopy has been also performed on these three materials and in Figure 13 (Nyquist diagram) the real and imaginary parts of impedance have been reported.

Table 5. Pseudo-diffusion coefficients D (in $\text{cm}^2 \cdot \text{s}^{-1}$).

Material (Symbol)	D ($\text{cm}^2 \cdot \text{s}^{-1}$)
LiFePO_4	2.0×10^{-14}
$\text{LiMn}_{0.05}\text{Fe}_{0.95}\text{PO}_4$	5.7×10^{-14}
$\text{LiMn}_{0.1}\text{Fe}_{0.9}\text{PO}_4$	7.7×10^{-14}

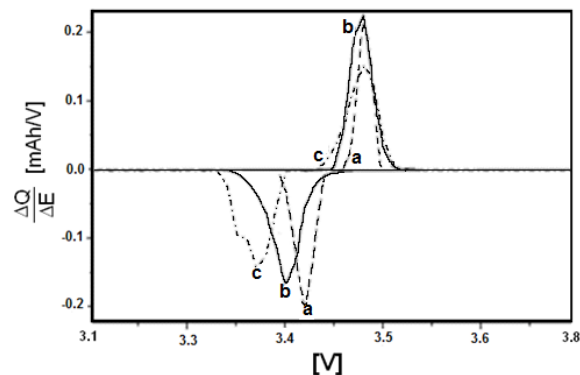


Figure 12. Potential spectroscopy of: (a) $\text{LiMn}_{0.1}\text{Fe}_{0.9}\text{PO}_4$; (b) $\text{LiMn}_{0.05}\text{Fe}_{0.95}\text{PO}_4$; and (c) LiFePO_4 .

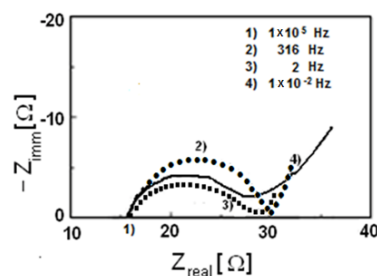


Figure 13. Impedance spectroscopy of: (a) • $\text{LiMn}_{0.1}\text{Fe}_{0.9}\text{PO}_4$; (b) – $\text{LiMn}_{0.05}\text{Fe}_{0.95}\text{PO}_4$; and (c) ■ LiFePO_4 .

The electrolytic resistance R_{el} is the first intercept of the semicircle with the x -axis, while the second intercept minus the electrolytic resistance R_{el} represents the charge transfer resistance R_{ct} . Therefore, it is possible to state that for all cases R_{ct} is about 15Ω . It is known by literature that the transfer charge resistance for pristine LiFePO_4 without in situ carbon formation is higher than $40\text{--}50 \Omega$ [33,34], so that by using this synthetic method a decrease of the charge transfer resistance has been, overall, reached.

Finally, we compared the synthesis and the electrochemical performances of our materials with analogous $\text{LiMn}_x\text{Fe}_{(1-x)}\text{PO}_4$ already described in the literature and reported in Table 6.

Table 6. Electrochemical performances of analogous $\text{LiMn}_x\text{Fe}_{(1-x)}\text{PO}_4$ material described in the literature.

Compound	Method	C-Rate	Capacity (mAh/g)	Reference
$\text{LiMn}_x\text{Fe}_{(1-x)}\text{PO}_4/\text{C}$ ($x = 0; 0.5; 1$)	Solvothermal process	C/5	150; 65; 50	[35]
$\text{LiMn}_x\text{Fe}_{(1-x)}\text{PO}_4/\text{C}$ ($x = 0; 0.5; 1$)	freeze-dry process	C/20	140; 120; 95	[36]
$\text{LiMn}_x\text{Fe}_{(1-x)}\text{PO}_4/\text{C}$ ($x = 0.7; 0.8; 0.9$)	Solid state reaction	C/10	110; 120; 130	[37]
$\text{LiMn}_x\text{Fe}_{(1-x)}\text{PO}_4$ ($x = 0; 0.05; 0.1; 0.2; 0.4$)	Hydrothermal process	C/10	140; 110; 95; 90; 78	[38]
$\text{LiMn}_x\text{Fe}_{(1-x)}\text{PO}_4$ ($x = 0; 0.1; 0.2; 0.3$)	Mechano-activation synthesis	C/10	135; 108; 125; 80	[39]

Saravanan et al. [35] produced $\text{LiMn}_x\text{Fe}_{(1-x)}\text{PO}_4/\text{C}$ ($x = 0; 0.5; 1$) with in situ carbon formation, by using the solvothermal method. They obtained a specific capacity equal to 150, 65, and 50 mAh/g for x equal to 0, 0.5 and 1, respectively, after 20 cycles at C/5. The same material obtained by Yoncheva et al. [36] at 500 °C starting from a phosphonate-formate precursor, freeze-drying an aqueous solution containing Li, Fe and Mn phosphate and formate ions, on the other hand, showed a capacity of 140, 120, and 95 mAh/g for x equal to 0, 0.5 and 1, respectively, a C/20. Zhang et al. [37] produced $\text{LiMn}_x\text{Fe}_{(1-x)}\text{PO}_4/\text{C}$ by solid state reaction with $x = 0.7, 0.8$, and 0.9 , obtaining at C/10 a capacity ranging from 110 to 130 mAh/g as x decreases. Xu et al. [38] synthesized carbon free materials through a direct hydrothermal process a 170 °C achieving a capacity of 140, 110, 95, 90, and 78 mAh/g for x

equal to 0.1, 0.2, 0.05, 0, and 0.4, respectively, at C/10. The lowest charge transfer resistance has been obtained for $x = 0.1$ and it is about $200\ \Omega$, while, for $x = 0.2$ and $x = 0$, it is 450 and $1400\ \Omega$, respectively.

Finally Wang et al. [39], which attained carbon-free $\text{LiMn}_x\text{Fe}_{(1-x)}\text{PO}_4$ by mechano-activation assisted synthesis, reached, the best performance of 125 mAh/g for x equal to 0.2 at C/10.

On the basis of these considerations, our results are consistent and, in some cases, even better than those found in the literature.

4. Experimental

SEM analysis were obtained by the high-resolution microscope FE-SEM Auriga-Zeiss. The apparatus is also equipped with an EDX (Energy Dispersive X-Ray) detector (Bruker, Milan, Italy). Room temperature powder X-ray diffraction was performed by using Cu-K α radiation $\lambda = 0.15418\ \text{nm}$ (Philips PW 1830 generator and Seifert XRD-3000 diffractometers). The data were collected with a step size of 0.02° and at count time of 4 s per step ($0.3^\circ \cdot \text{min}^{-1}$) over the range $15^\circ \leq 2\theta \leq 80^\circ$. The powder diffraction pattern was indexed by using a Rietveld profile analysis [40].

Thermogravimetric (DSC-TGA) data of the precursor mixtures were obtained in flowing dry nitrogen at a heating rate of $10\ ^\circ\text{C}\cdot\text{min}^{-1}$ on a TA Instruments SDT Q600 thermogravimetric analysis. The FT-IR absorption spectra were recorded on a Shimadzu Prestige 21 FT-IR spectrophotometer using KBr pellets. BET (Fisons Instruments) analyses have been performed at liquid nitrogen temperature and using gaseous N₂ to evaluate the specific surface of powders. Elemental analysis has been performed by the Servizio di Microanalisi del ISM-CNR, Monterotondo, Rome, Italy. Electrochemical characterization of samples was performed in T-shaped battery cells with lithium metal as counter (anode) and reference electrode. The cathode electrode contains about 10 mg of electroactive material with 10 wt % of Carbon Super S and 5 wt % of Teflon. The electrolyte is constituted by a glass wool separator filled with a 1 M solution of LiPF₆ in 1/1 ethylene carbonate/diethyl carbonate. Potential step voltammetry (PSV) was carried out in a three-electrode cell configuration by using the following setting values: potential step: 0.02 V, relaxation time: 10 min, step duration: until $I > I_0/30$ or 10 s if $I_0 < 0.01\ \text{mA}$ and in the range 3.2–3.7 V versus lithium. The same configuration was used for the potentiostatic–intermittent titration technique (PITT) experiments. The electrochemical impedance spectroscopy (EIS) has been performed in a frequency range from 10^5 to $10^{-2}\ \text{Hz}$, with a voltage amplitude of 0.01 V applied on a cell voltage of 3.47 V. A frequency response analyzer (Solartron 1255 HF and Solartron 1286 models by EG and G) and a galvanostat–potentiostat (Mac-Pile II Biologic) were used for these experiments.

5. Conclusions

Hybrid organic-inorganic precursors based on metal(II) phenylphosphonates have been synthesized, characterized and used for the synthesis of different $\text{LiFe}_{(1-x)}\text{Mn}_x\text{PO}_4$ composites. First of all, $\text{LiMn}_{0.1}\text{Fe}_{0.9}\text{PO}_4$ has been prepared following two different synthetic routes, i.e., using as organic precursors either $\text{Fe}_{0.9}\text{Mn}_{0.1}(\text{C}_6\text{H}_5\text{PO}_3)\cdot\text{H}_2\text{O}$ (**P1** precursor) or a mixture of $\text{Fe}(\text{C}_6\text{H}_5\text{PO}_3)\cdot\text{H}_2\text{O}$ and $\text{Mn}(\text{C}_6\text{H}_5\text{PO}_3)\cdot\text{H}_2\text{O}$ (**P2** and **P3** precursors). The materials thus obtained show similar behaviour, even if the sample prepared by using a mixture of **P2** and **P3** precursors presents a slightly higher capacity and seems to be more stable upon cycling. Subsequently, a series of $\text{LiMn}_{(1-x)}\text{Fe}_x\text{PO}_4$ (with $x = 0.05, 0.1, 0.5, 0.9$ and 0.95) has been produced by using only **P2**, **P3**, and Li_2CO_3 precursors mixtures. Structural and morphological characterizations have been carried out analysing the effect of the reciprocal presence of iron and manganese on the electrochemical performances. Enhancing the manganese content, the capacity decreases remarkably and the only advantage is the presence of a second charge-discharge plateau with higher potential value. Moreover, the reversibility degree of the insertion-deinsertion process increases, the pseudo-diffusion lithium coefficient increases only slightly and the charge transfer resistance almost keeps constant, being in every cases quite lower than the corresponding values reported in literature for pristine LiFePO_4 . This is due to the presence of

carbon produced in situ during the synthesis, which seems to be the only component able to increase substantially the electrochemical performances of this cathode material.

Author Contributions: M.P. conceived and designed the experiments; A.D. and E.M.B. performed the experiments; A.D., E.M.B., S.V.C., F.A.S. and C.L. analysed the data; and A.D. and S.V.C. wrote the paper.

Conflicts of Interest: The authors declare no conflict of interest.

References

1. Lu, L.; Han, X.; Li, J.; Hua, J.; Ouyang, M. A review on the key issues for lithium-ion battery management in electric vehicles. *J. Power Sources* **2013**, *226*, 272–288. [[CrossRef](#)]
2. Mathew, M.; Kong, Q.H.; McGrory, J.; Fowler, M. Simulation of lithium ion battery replacement in a battery pack for application in electric vehicles. *J. Power Sources* **2017**, *349*, 94–104. [[CrossRef](#)]
3. Pelletier, S.; Jabali, O.; Laporte, G.; Veneroni, M. Battery degradation and behaviour for electric vehicles: Review and numerical analyses of several models. *Trans. Res. Part B Methodol.* **2017**, *103*, 158–187. [[CrossRef](#)]
4. Olivetti, E.A.; Ceder, G.; Gaustad, G.G.; Fu, X. Lithium-Ion Battery Supply Chain Considerations: Analysis of Potential Bottlenecks in Critical Metals. *Joule* **2017**, *1*, 229–243. [[CrossRef](#)]
5. Santiangeli, A.; Fiori, C.; Zuccari, F.; Dell’Era, A.; Orecchini, F.; D’Orazio, A. Experimental analysis of the auxiliaries consumption in the energy balance of a pre-series plug-in hybrid-electric vehicle. *Energy Procedia* **2014**, *45*, 779–7868. [[CrossRef](#)]
6. Orecchini, F.; Santiangeli, A.; Dell’Era, A. EVs and HEVs Using Lithium-Ion Batteries. In *Lithium-Ion Batteries: Advances and Applications*; Pistoia, G., Ed.; Elsevier B.V.: Amsterdam, The Netherlands, 2014; pp. 205–248. ISBN 978-044459513-3. [[CrossRef](#)]
7. Fabbri, G.; Mascioli, F.M.F.; Pasquali, M.; Mura, F.; Dell’Era, A. Automotive application of lithium-ion batteries: A new generation of electrode materials. In Proceedings of the IEEE 22nd International Symposium on Industrial Electronics (ISIE), Taipei, Taiwan, 28–31 May 2013. [[CrossRef](#)]
8. Dell’Era, A.; Pasquali, M.; Fabbri, G.; Pasquali, L.; Tarquini, G.; Santini, E. Automotive application of lithium-ion batteries: Control of commercial batteries in laboratory test. In Proceedings of the IEEE 23rd International Symposium on Industrial Electronics (ISIE), Istanbul, Turkey, 1–4 June 2014; pp. 1616–1621. [[CrossRef](#)]
9. Fergus, J. Recent Developments in Cathode Materials for Lithium Ion Batteries. *J. Power Sources* **2010**, *195*, 939–954. [[CrossRef](#)]
10. Scrosati, B.; Garche, J. Lithium Batteries: Status, Prospects and Future. *J. Power Sources* **2010**, *195*, 2419–2430. [[CrossRef](#)]
11. Li, Z.; Zhang, D.; Yang, F. Developments of Lithium Ion Batteries and Challenges of LiFePO₄ as One Promising Cathode Material. *J. Mater. Sci.* **2009**, *44*, 2435–2443. [[CrossRef](#)]
12. Padhi, A.K.; Nanjundaswamy, K.S.; Goodenough, J.B. Phospho_Olivines as Positive_Electrode Materials for Rechargeable Lithium Batteries. *J. Electrochem. Soc.* **1997**, *144*, 1188–1194. [[CrossRef](#)]
13. Bauer, E.M.; Bellitto, C.; Righini, G.; Pasquali, M.; Dell’Era, A.; Prosini, P.P. A versatile method of preparation of carbon-rich LiFePO₄: A promising cathode material for Li-ion batteries. *J. Power Sources* **2005**, *146*, 544–549. [[CrossRef](#)]
14. Pasquali, M.; Dell’Era, A.; Prosini, P.P. Fitting of the voltage-Li + insertion curve of LiFePO₄. *J. Solid State Electrochem.* **2009**, *13*, 1859–1865. [[CrossRef](#)]
15. Benoit, C.; Franger, S. Chemistry and Electrochemistry of Lithium Iron Phosphate. *J. Solid State Electrochem.* **2008**, *12*, 987–993. [[CrossRef](#)]
16. Dell’era, A.; Pasquali, M. Comparison between different ways to determine diffusion coefficient and by solving Fick’s equation for spherical coordinates. *J. Solid State Electrochem.* **2009**, *13*, 849–859. [[CrossRef](#)]
17. Safronov, D.V.; PinusI, Y.; Profatilova, I.A.; Tarnopolskii, V.A.; Skundin, A.M.; Yaroslavtsev, A.B. Kinetics of Lithium Deintercalation from LiFePO₄. *Inorg. Mater.* **2011**, *47*, 303–307. [[CrossRef](#)]
18. Barker, J.; Saidi, M.Y.; Swoyer, J.L. Lithium Iron(II) Phospho-olivines Prepared by a Novel Carbothermal Reduction Method. *Electrochim. Solid-State Lett.* **2003**, *6*, A53–A55. [[CrossRef](#)]
19. Wang, D.; Li, H.; Shi, S.; Huang, X.; Chen, L. Improving the Rate Performance of LiFePO₄ by Fe_Site Doping. *Electrochim. Acta* **2005**, *50*, 2955–2958. [[CrossRef](#)]

20. Roberts, M.R.; Vitins, G.; Owen, J.R. High Throughput Studies of $\text{Li}_{1-x}\text{Mg}_x/2\text{FePO}_4$ and $\text{LiFe}_{1-y}\text{Mg}_y\text{PO}_4$ and the Effect of Carbon Coating. *J. Power Sources* **2008**, *179*, 754–762. [CrossRef]
21. Wang, G.X.; Bewlaiy, S.L.; Konstantinov, K.; Liu, H.K.; Dou, S.X.; Ahn, J.H. Physical and electrochemical properties of doped lithium iron phosphate electrodes. *Electrochim. Acta* **2004**, *50*, 443–447. [CrossRef]
22. Safronov, D.V.; Novikova, S.A.; Kulova, T.L.; Skundin, A.M.; Yaroslavtsev, A.B. Lithium Diffusion in Materials Based on LiFePO_4 Doped with Cobalt and Magnesium. *Inorg. Mater.* **2012**, *48*, 513–519. [CrossRef]
23. Nakamura, T.; Sakumoto, K.; Okamoto, M.; Seki, S.; Kobayashi, Y.; Takeuchi, T.; Tabuchi, M.; Yamada, Y. Electrochemical study on Mn^{2+} substitution in LiFePO_4 olivine compound. *J. Power Sources* **2007**, *174*, 435–441. [CrossRef]
24. Nakamura, T.; Miwa, Y.; Tabuchi, M.; Yamada, Y. Structural and Surface Modifications of LiFePO_4 Olivine Particles and Their Electrochemical Properties. *J. Electrochem. Soc.* **2006**, *153*, A1108–A1114. [CrossRef]
25. Lee, K.T.; Lee, K.S. Electrochemical properties of $\text{LiFe}0.9\text{Mn}0.1\text{PO}_4/\text{Fe}_2\text{P}$ cathode material by mechanical alloying. *J. Power Sources* **2009**, *189*, 435–439. [CrossRef]
26. Altomare, A.; Bellitto, C.; Ibrahim, S.A.; Mahmoud, M.R.; Rizzi, R. Iron(ii) phosphonates: A new series of molecule-based weak ferromagnets. *J. Chem. Soc. Dalton Trans.* **2000**, *21*, 3913–3919. [CrossRef]
27. Bellitto, C.; Federici, F.; Colapietro, M.; Portalone, G.; Caschera, D. X-ray single-crystal structure and magnetic properties of $\text{Fe}[\text{CH}_3\text{PO}_3]\cdot\text{H}_2\text{O}$: A layered weak ferromagnet. *Inorg. Chem.* **2002**, *41*, 709–714. [CrossRef]
28. Bauer, E.M.; Bellitto, C.; Pasquali, M.; Prosini, P.P.; Righini, G. Versatile synthesis of carbon-Rich LiFePO_4 enhancing its Electrochemical Properties. *Electrochim. Solid-State Lett.* **2004**, *7*, A85–A87. [CrossRef]
29. Ho, C.; Raistrick, I.D.; Huggins, R.A. Application of A-C techniques to the study of lithium diffusion in tungsten trioxide thin films. *J. Electrochem. Soc.* **1980**, *127*, 343–350. [CrossRef]
30. Levi, M.D.; Levi, E.A.; Aurbach, D. The mechanism of lithium intercalation in graphite film electrodes in aprotic media Part 2 potentiostatic intermittent titration and in situ XRD studies of the solid-state ionic diffusion. *J. Electroanal. Chem.* **1997**, *421*, 89–97. [CrossRef]
31. Weppner, W.; Huggins, R.A. Determination of the kinetic parameter of mixed-conducting electrodes and application to the system Li_3Sb . *J. Electrochem. Soc.* **1977**, *1569*–1578. [CrossRef]
32. McKinnon, W.R.; Haering, R.R. *Modern Aspect in Electrochemistry*, 1st ed.; White, R.E., Bockris, J.O.M., Conway, B.E., Eds.; Plenum Press: New York, NY, USA; London, UK, 1983; ISBN 978-1-4615-7463-7. [CrossRef]
33. Wang, C.; Hong, J. Ionic/Electronic Conducting Characteristics of LiFePO_4 Cathode Materials. The Determining Factors for High Rate Performance. *Electrochim. Solid-State Lett.* **2007**, *10*, A65–A69. [CrossRef]
34. Park, C.Y.; Park, S.B.; Oh, S.H.; Jang, H.; Cho, W.I.; Ion, L. Diffusivity and Improved Electrochemical Performances of the Carbon Coated LiFePO_4 . *Bull. Korean Chem. Soc.* **2011**, *32*, 836–840. [CrossRef]
35. Saravanan, K.; Vitta, J.J.; Reddy, M.V.; Chowdari, B.V.R.; Balaya, P. Storage performance of $\text{LiFe}_{1-x}\text{Mn}_x\text{PO}_4$ nanoplates ($x = 0, 0.5$, and 1). *J. Solid State Electrochem.* **2010**, *14*, 1755–1760. [CrossRef]
36. Yoncheva, M.; Koleva, V.; Mladenov, M.; Sendova-Vassileva, M.; Nikolaeva-Dimitrova, M.; Stoyanova, R.; Zhecheva, E. Carbon-coated nano-sized $\text{LiFe}_{1-x}\text{Mn}_x\text{PO}_4$ solid solutions ($0 \leq x \leq 1$) obtained from phosphate-formate precursors. *J. Mater. Sci.* **2011**, *46*, 7082–7089. [CrossRef]
37. Xu, J.; Chen, G.; Li, H.J.; Lv, Z.S. Direct-hydrothermal synthesis of $\text{LiFe}_{1-x}\text{Mn}_x\text{PO}_4$ cathode materials. *J. Appl. Electrochem.* **2010**, *40*, 575–580. [CrossRef]
38. Zhang, B.; Wang, X.; Li, H.; Huang, X. Electrochemical performances of $\text{LiFe}_{1-x}\text{Mn}_x\text{PO}_4$ with high Mn content. *J. Power Sources* **2011**, *196*, 6992–6996. [CrossRef]
39. Wang, Y.; Zhang, D.; Yu, X.; Cai, R.; Shao, Z.; Liao, X.Z.; Ma, Z.F. Mechanoactivation-assisted synthesis and electrochemical characterization of manganese lightly doped LiFePO_4 . *J. Alloy. Compd.* **2010**, *492*, 675–680. [CrossRef]
40. Rietveld, H.M. A profile refinement method for nuclear and magnetic structures. *J. Appl. Crystallogr.* **1969**, *2*, 65–71. [CrossRef]

